Rock Mechanics and Rock Engineering

Estimation of fracture toughness of anisotropic rocks by semi-circular bend (SCB) test under water vapor pressure

--Manuscript Draft--

Manuscript Number:	
Full Title:	Estimation of fracture toughness of anisotropic rocks by semi-circular bend (SCB) test under water vapor pressure
Article Type:	Original Paper
Keywords:	Anisotropic rock; Fracture; Fracture toughness; Semi-Circular Bend (SCB) test; Water vapor pressure; X-ray CT method
Corresponding Author:	Minami Kataoka Kumamoto University Kumamoto, JAPAN
Corresponding Author Secondary Information:	
Corresponding Author's Institution:	Kumamoto University
Corresponding Author's Secondary Institution:	
First Author:	Minami Kataoka
First Author Secondary Information:	
Order of Authors:	Minami Kataoka
	Yuzo Obara, PhD
	Mahinda Kuruppu, PhD
Order of Authors Secondary Information:	
Abstract:	In order to investigate the influence of water vapor pressure in surrounding environment on mode I fracture toughness (KIC) of rocks, Semi-Circular Bend (SCB) tests under various water vapor pressures were conducted. The water vapor is the most effective agent which promotes stress corrosion of rocks. The range of the water vapor pressure used in this test was 10-2 to 103 Pa. Two kinds of an anisotropic rock, African granodiorite and Korean granite were used. Measurement of elastic wave velocity and observation of thin sections of these rocks were performed to investigate the micro structures of the rocks. It was found that the distribution of inherent micro cracks and grains have a preferred orientation. Two types of specimens in different orientations, namely Type-1 and Type-3 were prepared based on the anisotropy identified by the differences of the elastic wave velocity. KIC of both the rocks is dependent on the water vapor pressure in the surrounding environment and decreases with increasing the water vapor pressure. It was found that the degree of the dependence is influenced by the orientation and density of inherent micro cracks. The experimental results also show that KIC depends on the material anisotropy. A fracture process was discussed on the basis of the geometry of fractures within fractured specimens visualized by X-ray CT method. It was concluded that the dominant factor causing the anisotropy of KIC is the distribution of grains rather than inherent micro cracks in these rocks.

Minami Kataoka, Yuzo Obara, Mahinda Kuruppu

Estimation of fracture toughness of anisotropic rocks by semi-circular bend (SCB) test under water vapor pressure

M. Kataoka
Kumamoto University, 2-39-1 Kurokami, Chuo-ku, Kumamoto 860-8555, Japan
Email: 127d9401@st.kumamoto-u.ac.jp
Tell: +81-96-342-3697

Y. Obara
Kumamoto University, 2-39-1 Kurokami, Chuo-ku, Kumamoto 860-8555, Japan

M. Kuruppu
Curtin University, Locked Bag 30, Kalgoorlie, WA 6433, Australia

Abstract

In order to investigate the influence of water vapor pressure in surrounding environment on mode I fracture toughness (K_{IC}) of rocks, Semi-Circular Bend (SCB) tests under various water vapor pressures were conducted. The water vapor is the most effective agent which promotes stress corrosion of rocks. The range of the water vapor pressure used in this test was 10^{-2} to 10^{3} Pa. Two kinds of an anisotropic rock, African granodiorite and Korean granite were used. Measurement of elastic wave velocity and observation of thin sections of these rocks were performed to investigate the micro structures of the rocks. It was found that the distribution of inherent micro cracks and grains have a preferred orientation. Two types of specimens in different orientations, namely Type-1 and Type-3 were prepared based on the anisotropy identified by the differences of the elastic wave velocity. K_{IC} of both the rocks is dependent on the water vapor pressure in the surrounding environment and decreases with increasing the water vapor pressure. It was found that the degree of the dependence is influenced by the orientation and density of inherent micro cracks. The experimental results also show that K_{IC} depends on the material anisotropy. A fracture process was discussed on the basis of the geometry of fractures within fractured specimens visualized by X-ray CT method. It was concluded that the dominant factor causing the anisotropy of K_{IC} is the distribution of grains rather than inherent micro cracks in these rocks.

Keywords

Anisotropic rock; Fracture; Fracture toughness; Semi-Circular Bend (SCB) test; Water vapor pressure; X-ray CT method

1. Introduction

Fracture for brittle materials is resulted through crack initiation and propagation, namely the fracture process. Crack initiation takes place when stress intensity factor K at a micro crack tip reaches a critical value, so-called the fracture toughness K_C. After the initiation, the fracture propagates and connects to other fractures, and finally the material reaches failure. The fracture toughness is one of the mechanical properties indicating resistance to crack initiation. It has been applied as (a) a parameter for classification of rock materials, (b) an index for rock fragmentation and (c) a material property in interpretation of geological features and in stability analysis of rock structures, as well as in modeling of fracturing of rocks (Whittaker et al. 1992). Estimation of the fracture toughness is important to understand brittle fracture behavior of rocks.

The fracture toughness of rocks is known to be affected by the surrounding environment. Many experiments have been conducted under various surrounding conditions, such as temperature, humidity, confining pressure (Meredith and Atkinson 1985; Al-shayea et al. 2000; Al-shayea 2002; Funatsu et al. 2004; Obara et al. 2006; Obara et al. 2007; Kataoka et al. 2011; Kataoka et al. 2012). Among these conditions, Obara et al. (2006; 2007) have focused on the effect of water vapor on the fracture toughness of rocks determined using Semi-Circular Bend (SCB) tests (Chong and Kuruppu 1984; Kuruppu et al. 2014) under various water vapor pressures. It was found that the fracture toughness of andesite and basalt is dependent on the water vapor pressure and decreases with increasing the water vapor pressure. This tendency is also shown in uniaxial compressive strength and tensile strength of rocks. Jeong et al. (2007) and Kataoka et al. (2013) concluded that this phenomenon occurred due to stress corrosion of rocks promoted by the water vapor in the surrounding environment. The stress corrosion is a chemical reaction activated by stress concentration at a micro crack tip (Freiman 1984; Atkinson 1987). Therefore it can be considered that the stress corrosion of rocks is affected by micro structure characteristics of rocks, such as density and orientation of inherent micro cracks, and kinds, size and distribution of mineral grains.

It is also considered that these micro structures induce anisotropy on physical properties of rocks. For example, crystalline rocks such as granite have anisotropic properties causing differences in elastic wave velocity, uniaxial compressive strength, tensile strength and fracture toughness in different directions (Lee et al. 2001; Nasseri 2008). The anisotropy can be attributed to the existence of preferred orientations of micro crack distribution (Schedl et al. 1986). As the micro crack distribution that supports microscopic crack initiation is influenced by the micro structure of rock, the fracture toughness seems to be affected by the micro structures. Accordingly, the influence of the micro structures on the anisotropy of the fracture toughness should be investigated.

Several tests were proposed to estimate mode I fracture toughness of rocks, namely Chevron Bend (CB) test (Ouchterlony 1980; ISRM Testing Commission 1988), Single Edge Cracked Round Bar in Bending test (Ouchterlony 1981), Short Rod (SR) test (Barker 1977; ISRM 1988), Central Straight Through Brazilian Disk test (Atkinson et al. 1982), Cracked Chevron Notched Brazilian Disk (CCNBD) test (Fowell and Chen 1990; ISRM 1995), SCB test and Straight Notched Disk Bending test (Tutluoglu and Keles 2011). The International Society for Rock Mechanics (ISRM) (1988; 1995) suggested CB, SR and CCNBD tests for the determination of static fracture toughness of rocks. SCB test has been added to the suggested method in 2014 (Kuruppu et al. 2014).

In this research, fracture toughness of two kinds of anisotropic rocks, African granodiorite (AG) (Kataoka et al. 2011; Kataoka et al. 2012) and Korean granite (KG) (Kataoka et al. 2012), was determined under various water vapor pressures and its dependence on the water vapor pressure of the surrounding environment was investigated.

SCB test was chosen to estimate the fracture toughness of the rocks for its simplicity of specimen preparation, equipment and testing procedure. Detailed observation of fractures within fractured specimens was performed after the SCB tests. The fracture process was discussed and the influence of the micro structure of the rock on the anisotropy of the fracture toughness examined.

2. Semi-Circular Bend (SCB) test

2.1 Outline

The geometry of SCB specimen is shown in Fig. 1. This test was developed by Chong and Kuruppu (1984). The specimen is a typical core-based and required very little machining. In particular, its compact shape required by cutting a core and duplicating a disc is suitable for investigation of the effect of various parameters such as strain rate, moisture content and temperature on the fracture toughness of rocks (Karfakis 1986). Mode I fracture toughness K_{IC} is estimated using a following equation (Kuruppu et al. 2014),

$$K_{IC} = \frac{P_{max}\sqrt{\pi a}}{2rt} Y_I \quad , \tag{1}$$

where a, r and t are an artificial notch length, radius and thickness of the specimen, respectively. P_{max} is a maximum load. The normalized stress intensity factor Y_I is dimensionless and given as a function of a dimensionless notch length a/r and a half of support span to radius ratio s/r (Kuruppu et al. 2014).

2.2 Experimental method

Setup of the specimen for the SCB test using a loading apparatus is shown in Fig. 2 (a). The specimen was placed on two lower support rollers with the support span width $2s$ shown in Fig. 1. The value of s/r is 0.8 in these tests. Load was applied through one upper and two lower rollers. A loading bar with a load cell can move up and down vertically aided by guide rods.

Fig. 2 (b) shows a vacuum chamber used to control the surrounding environment of the specimen. The chamber, which is made of SUS304 steel, has upper and lower flanges, ports and a valve for injection of gases or vapors. One of the ports was used to lead output from the load cell. Another two ports were used to measure the water vapor pressure in the chamber by two types of pressure gauges and one port with a valve was connected to an evacuation system as described below.

The specimen was placed inside the vacuum chamber as shown in Fig. 2 (b) and the chamber was placed at a MTS servo-controlled testing machine with a capacity of 100 kN as shown in the bottom right of Fig. 2. The chamber has flanges with a loading rod and the specimen was loaded by pressing down the upper flange using the testing machine. The load application was controlled by a constant displacement rate of 0.01 mm/min. The flanges of the chamber are supported by two steel columns with springs as shown in Fig. 2 (b). These springs prevent any load application on the specimen while the surrounding environment was controlled by a process mentioned below. The load was recorded using the load cell with a capacity of 10 kN equipped at the loading bar shown in Fig. 2 (a). The displacement at the upper loading point was measured using a transducer of the testing machine.

It is necessary that the air in the chamber was exhausted and that various quantities of water vapor were provided. The chamber is linked to the evacuation system through a flexible tube as shown in Fig. 2 (c) during the test. It consists of two vacuum pumps: a rotary pump and a turbo molecular pump. The water vapor pressure in the chamber was measured using two pressure gauges as shown in Fig. 2 (b), namely Pirani pressure gauge with a measurement range of 10^{-1} to 10^{5} Pa and Penning pressure gauge with the range of 10^{-6} to 10^{0} Pa. Fig. 3 shows the change of the pressure in the chamber before and during the loading. At first, the air in the chamber was exhausted using two pumps until the pressure declined to lower than 10^{-2} Pa. Then the distilled water was injected through the injection valve to a pressure of about 10^{3} Pa. As a result, the pressure in the chamber became the saturated water vapor pressure at the room temperature and the chamber was filled with only water vapor. It is considered that the air in the chamber was fully changed to the new environment, namely the water vapor environment. Finally the water vapor in the chamber was exhausted again to a required pressure using the evacuation system. Having the required water vapor pressure maintained for about six hours, the SCB test was carried out.

3. Specimen

African granodiorite (AG) and Korean granite (KG) were used as test materials in this research.

3.1 Preparation of specimens

The rock blocks shown in Fig. 4 were measured for elastic wave velocity v_p in three normal directions. Table 1 shows the results of the measurement and three directions were defined as Axis-1, Axis-2 and Axis-3 in order of decreasing v_p. Planes perpendicular to each axis were also defined as Plane-1, Plane-2 and Plane-3 as shown in Fig. 5. As the results, v_p in the direction of Axis-1 is higher than that in the other two directions. The direction of higher v_p has lower resistance to the elastic wave propagation. Therefore many of the inherent micro cracks may be oriented to Axis-1 and Axis-2 as shown in Fig. 5.

A rock core with a diameter of 75 mm was drilled to the direction of Axis-2 of the blocks as shown in Fig. 6. Then the core was sliced into disks with a thickness of approximately 20 mm and each disk was cut into halves to form two semi-circular specimens. Finally an artificial notch was produced using a diamond blade with a thickness of 0.4 mm. The length of the notch is given by $a/r = 0.5$ where a and r are defined in Fig. 1. The corresponding value of Y_I in Eq. (1) is approximately 6.65. In this paper, two types of specimen were prepared, Type-1 and Type-3 as shown in Fig. 6. The number of the type name represents the direction of the artificial notch and the loading during the test.

The water within specimens should be removed to investigate the influence of the water vapor pressure on the fracture toughness of the rocks. In order to achieve complete dry condition of the specimens, they were kept in an electric drying oven at 100 ^{o}C for more than 30 days before the tests.

3.2 Investigation of micro structures

In order to investigate the micro structures of rocks, observation of thin sections was performed using a polarization microscope. The thin sections were prepared from three planes: Plane-1, Plane-2 and Plane-3. Fig. 7 shows micrographs of the thin sections of both rocks in Plane-2. Mineral grains of plagioclase, amphibole and biotite,

and quartz, alkali feldspar and biotite are observed in AG and KG, respectively.

In order to measure the distribution of micro cracks in each plane, their density in a particular direction, namely the number per unit area, is drawn in a rose diagram sequentially at intervals of 20 degrees as shown in Fig. 8. Many micro cracks are oriented to the direction of Axis-1 and Axis-2 for AG as the micro crack density in these directions is higher. The tendency of the results is the same as that of the estimation by the elastic wave velocity measurement described in Section 3.1. The micro crack density in KG also varies in different principal directions, namely the density of micro cracks aligned in the direction of Axis-1 and Axis-2 is higher than that of Axis-3. In addition, the micro crack density in KG is lower than that in AG on the whole and almost the same as the density of micro cracks oriented to the direction of Axis-3 in AG (the direction of lower micro crack density).

Intercept method (ASTM 2010) was used to estimate an average grain diameter d in three directions. This method consists of drawing a line on the micrographs and counting the number of grains intercepted by the line. The length of the line divided by the number of the intercepted grains gives the average grain diameter d. It was applied to each plane and each direction of axes. The results are shown in Table 2. Result for AG reveal that d in the direction of Axis-3 is larger than those in Plane-1 and Plane-2, and that d in Axis-1 and Axis-2 directions is almost the same in Plane-3. While KG has smaller differences of d in various directions than AG, d in the direction of Axis-3 tends to be larger. It shows that the long axes of grains are oriented to the direction of Axis-3. Therefore the geometry of grain boundaries in the direction of Axis-3 is straighter than that of Axis-1. In addition, d of AG is larger than that of KG.

4. Results

The SCB test results and the conditions under which they were performed for both rocks are summarized in Tables 3 and 4. A series of tests was performed using 11 and 14 specimens for Type-1 and Type-3 of African granodiorite (AG), and 17 and 15 specimens for Type-1 and Type-3 of Korean granite (KG), respectively. The range of the water vapor pressure p in these tests was from 1.0×10^{-2} to 7.7×10^{2} Pa. The fracture toughness K_{IC} is estimated from the maximum load P_{max} using Eq. (1) described in Section 2.

Fig. 9 shows examples of load-displacement curves. In these figures, the curves of both types are in the same graph and that of Type-3 is translated 0.1 mm in positive directions of horizontal axis. These curves are downward convex at a low load level and linear until a specimen fractured at P_{max}.

In order to investigate the initiation of the fracture, a SCB test was performed at atmospheric condition with Acoustic Emission (AE) monitoring. A specimen of AG Type-3 was used for this test. An AE sensor was attached to a side surface of the specimen. The AE signals were amplified by 40 dB and recorded by a computer with appropriate software (AEwin manufactured by Physical Acoustics Corporation). A threshold of 45 dB was selected and a band pass filter with a range of 100 kHz to 2 MHz was used. The load and AE event rate during the test are shown in Fig. 10 (a) and (b). In Fig. 10 (b), the load and displacement are normalized by the maximum load P_{max} and a displacement at P_{max}, respectively and drawn on a magnified scale, showing grey areas in Fig. 10 (a). The AE events are rarely recorded until the load at 97.5 % of P_{max} and the AE rate rises rapidly after the load leaches P_{max}. This result shows that the fracture initiates near P_{max} and propagates rapidly just after the initiation. Therefore P_{max} indicates the loading condition at the fracture initiation and can be used for the estimation of K_{IC} as the critical value of stress intensity factor K_I in the SCB test.

The relation between the fracture toughness K_{IC} and the water vapor pressure p is shown in Fig. 11 (refer to Tables 3 and 4). K_{IC} of both the rocks and of the two types investigated in each was plotted against the water vapor pressure p on the logarithmic graph and shown to decrease with increasing p. Lines drawn using least square approximation are also shown in this figure. The equation of the line is represented as:

$$K_{IC} = \beta p^{-m}, \quad (2)$$

where β is a constant and indicates K_{IC} at p = 1 Pa on this line. m is a slope of the line on the logarithmic graph and indicates the degree of the dependence of p on K_{IC}. These values are summarized in Table 5. The m value of AG Type-1 is higher than the others. Therefore the influence of p on K_{IC} for AG Type-1 is the strongest.

Results further show that the two rocks exhibit anisotropy of K_{IC} in varying degrees. While many micro cracks are oriented in the direction of Axis-1, K_{IC} of Type-1 is higher than that of Type-3 at the same pressure for the both rocks. It is well known that preferentially oriented micro cracks result in lower mechanical strength in that direction for rocks. The lower K_{IC} direction expected based on this knowledge (Axis-1) does not agree with the results that gives lower value for Type-3 where many micro cracks are aligned with Axis-1.

5. Discussion

5.1 Dependence of fracture toughness on water vapor pressure

The fracture toughness K_{IC} is dependent on the water vapor pressure p and decreases with increasing p for both rocks. This tendency is the same as K_{IC} of two kinds of volcanic rock, Kumamoto andesite and Kunnum basalt (Obara et al. 2006; Obara et al. 2007). The decrease of K_{IC} is due to stress corrosion promoted by water vapor in the surrounding environment. It is concluded that K_{IC} of rocks is influenced by the stress corrosion.

The m value, the degree of the dependence of p on K_{IC}, of African granodiorite (AG) Type-1 is higher than the others as shown in Table 5. As given in Section 3 and shown in Fig. 8 (AG), the micro crack density in the direction of Axis-1 is higher than that of Axis-3 for AG. Micro cracks aligned in a preferential direction give rise to planes of weakness in rocks. The effect of stress corrosion cracking on such planes can be more severe and the resistance to the fracture initiation decreases gradually with increasing the water vapor pressure p. Therefore the m value of Type-1 is higher than that of Type-3 for AG. On the other hand, the m values of Type-1 and Type-3 are almost the same for Korean granite (KG). This rock has lower micro crack density than AG as shown in Fig. 8 and smaller differences in directions. In addition, the micro crack density of KG is almost the same as that of AG in the direction of Axis-3. Therefore the m values of KG Type-1 and Type-3, and AG Type-3 are similar to each other. It is found that the m value is dependent on the orientation and the density of micro cracks and that the degree of stress corrosion has sensitivity to the micro crack distribution.

5.2 Anisotropy of fracture toughness

The rocks used in these tests exhibit anisotropy of the fracture toughness K_{IC}. The K_{IC} of Type-1 is higher than that of Type-3 at the same water vapor pressure p. The fracture initiates at the maximum load P_{max} and propagates after reaching P_{max} as described in Section 4. It means that K_{IC} corresponds to the point of fracture initiation occurring at the artificial notch tip. Therefore the fracture geometry observed near the artificial notch tip may be

considered and related to the fracture initiation of rock.

Following the SCB test, fractured specimens of AG Type-1 and Type-3 were scanned to visualize fractures within the specimens by micro-focus X-ray CT (Mukunoki 2013). The gray-level CT images of both types of specimens are shown in Fig. 12. The CT images were obtained as cross sections located at (a) 1.0 mm, (b) 0.5 mm and (c) 0.1 mm distance from the artificial notch tip and parallel to the notch front as shown at the bottom of Fig. 12. The images of Type-1 and Type-3 correspond to those taken in Plane-1 and Plane-3, respectively. In CT images, the dark region shows the area of low density, while the region of relatively light color shows that of high density. The black lines in these images show the gaps, namely the fractures. Traces of the fractures are also shown in this figure. Grain distributions are also observed in the CT images identified by the difference of density of each mineral. It is found that some parts of the fractures within Type-1 avoid going across grains with higher density and therefore the fractures are winding. On the other hand, the geometry of the fractures within Type-3 is straighter than that within Type-1.

As described in Section 3, the average grain diameter d in the direction of Axis-3 is larger. It means that the geometry of grain boundaries in the direction of Axis-3 is straighter than the others for AG. In the CT images of Type-1 as shown in the left of Fig. 12 (Plane-1), the fractures are oriented in the direction of Axis-2, namely perpendicular to straighter grain boundaries (Axis-3). These fractures are more winding than those within Type-3 shown in the right of this figure (Plane-3). From this observation of the fracture geometry, it can be found that the fracture tends to initiate along grain boundaries and avoid going through higher density grains, that is, the resistance to the fracture initiation across higher density grains is higher than if the fractures were to propagate along grain boundaries. Therefore the fracture toughness K_{IC} has anisotropic properties and K_{IC} of Type-1 is higher than that of Type-3 for AG. It is concluded that K_{IC} is remarkably dependent on the distribution and orientation of grains rather than that of micro cracks in this rock.

The fracture geometry observed on side surfaces of all fractured specimens was also considered. Figs. 13 and 14 show traces of the fractures. They were obtained by tracing the fractures on the photographs of the specimens. The fracture traces of both side surfaces are superposed in these figures. Dashed lines which are aligned with the directions of artificial notches are also shown. Angles of the fractures from 0 mm to 5 mm distance from the notch tips that make with the lines were measured. Table 6 shows the results of the measurement. The average fracture angle and the standard deviation of Type-1 are larger than those of Type-3 for both rocks.

The fractures can be expected to propagate in the direction of the artificial notch. According to the results, smaller fracture angle of Type-3 shows that many of the fractures propagate roughly in the expected direction, namely along the dashed line. On the other hand, the fracture angle of Type-1 is larger as the fractures propagate away from the dashed line more than that in Type-3. This fracture geometry may be conducive to the existence of greater resistance to fracture propagation in the direction of the artificial notch (Axis-1). As described in Section 3, the average grain size in the direction of Axis-3 is larger than that of Axis-1 and the fractures hardly propagate across grains resulting in increase of fracture resistance. In the case of Type-3, the fracture propagation is along the lengthwise direction of the grains (Axis-3) and experiences lower resistance than in Type-1. Therefore K_{IC} of Type-1 is higher than that of Type-3 because the Type-1 fracture needs more energy to initiate and propagate. This also supports the conclusion that K_{IC} is dependent on the grain orientation in the rocks used in these tests.

In order to confirm the discussion described above, K_{IC} in micro scale should be estimated. It is useful to develop a new laboratory test which can estimate K_{IC} of mineral grains and grain boundaries, namely microscopic K_{IC}

(Kataoka et al. 2014). In addition, numerical simulations of the fracture process are also needed along with the estimated microscopic K_{IC} in order to investigate the influence of micro structures on the macroscopic K_{IC} of rocks.

6. Conclusions

The fracture toughness of the crystalline rocks and the environment sensitivity to water vapor were investigated. Firstly the measurement of elastic wave velocity and the observation of thin sections were performed in the two kinds of anisotropic rocks, African granodiorite and Korean granite. Then a series of SCB tests were performed under various water vapor pressures to investigate the influence of the water vapor pressure on the fracture toughness of them. Furthermore, the fracture within the fractured specimen was observed using X-ray CT method following the SCB test. Finally the influence of micro structures on the anisotropy of the fracture toughness was discussed on the basis of the geometry of the observed fractures. The results are summarized as follows:

1) The preferred orientation of the inherent micro crack and grain distributions can be estimated by the measurement of elastic wave velocity and the observation of the thin sections of the rocks.
2) The fracture toughness K_{IC} of both the rocks is dependent on the water vapor pressure p and decreases with increasing p. The relation between K_{IC} and p is represented as:

$$K_{IC} = \beta p^{-m},$$

where m indicates the degree of the dependence of p on K_{IC}.
3) The decrease of K_{IC} occurred due to stress corrosion promoted by water vapor in the surrounding environment.
4) The m value is dependent on the orientation and density of inherent micro cracks.
5) The rock properties of elastic wave velocity and fracture toughness displayed anisotropy.
6) On the basis of the fracture geometry visualized by X-ray CT method, it was suggested that K_{IC} is dependent on the micro structure of each material. The grain distribution induces anisotropy of K_{IC} in the rocks tested.

References

Al-shayea NA (2002) Comparing reservoir and outcrop specimens for mixed mode I-II fracture toughness of a limestone rock formation at various conditions. Rock Mech Rock Eng 35(4): 271-91

Al-shayea NA, Khan K, Abduljauwad SN (2000) Effects of confining pressure and temperature on mixed-mode (I-II) fracture toughness of a limestone rock. Int J Rock Mech Min Sci 37: 629-43

ASTM Subcommittee (2010) ASTM E112-10 Standard test methods for determining average grain size. ASTM, Philadelphia

Atkinson BK (1987) Fracture Mechanics of Rock, academic press geology series. Academic Press, San Diego

Atkinson C, Smelser RE, Sanchez J (1982) Combined mode fracture via the cracked Brazilian disk test. Int J Fract 18: 4: 279-291

Barker LM (1977) A simplified method for measuring plane-strain fracture toughness. Eng Fract Mech 9: 361-369

Chong KP, Kurruppu MD (1984) New specimen for fracture toughness determination for rock and other materials. Int J Fract 26: 59-62

Fowell R J, Chen JF (1990) The third chevron-notched rock fracture specimen - the cracked chevron-notched Brazilian disc. Proc 31st US Rock Mech Symp, Balkema: 295-302

Freiman SW (1984) Effects of chemical environments on slow crack growth in glasses and ceramics. J Geophys Res 89: 4072-4076

Funatsu T, Seto M, Shimada H, Matsui K, Kuruppu M (2004) Combined effects of increasing temperature and confining pressure on the fracture toughness of clay bearing rocks. Int J Rock Mech Min Sci 41(6): 927-938

ISRM Testing Commission (1988) Suggested methods for determining the fracture toughness of rock. Int J Rock Mech Min Sci Geomech Abstr 25: 71-96

ISRM Testing commission (1995) Suggested method for determining mode I fracture toughness using cracked chevron notched Brazilian disk (CCNBD) specimens. Int J Rock Mech Min Sci Geomech Abstr 32: 57-64

Jeong HS, Kang SS, Obara Y (2007) Influence of surrounding environments and strain rates on strength of rocks under uniaxial compression. Int J Rock Mech Min Sci 44: 321-331

Karfakis MG (1986) Acritical review of fracture mechanics to hydraulic fracturing stress measurements. Proc SEM Spring Conf on Expl Mech: 141-147

Kataoka M, Hashimoto A, Sato A, Obara Y (2012) Fracture toughness of anisotropic rocks by semi-circular bend (SCB) test under water vapor pressure. Proc 7th ARMS, Seoul: 458-465

Kataoka M, Ito T, Takashima K, Obara Y (2014) A new testing method to estimate microscopic fracture toughness of rock. Proc ROCKMEC XIth Regional Rock Mech Sym, Afyonkarahisar (in press)

Kataoka M, Obara Y (2013) Estimation of fracture toughness of different kinds of rocks under water vapor pressure by SCB test. J MMIJ 129: 425-432 (in Japanese)

Kataoka M, Obara Y, Jeong HS (2013) Influence of water vapor pressure in surrounding environment on strength and fracture toughness of rocks. Proc ISRM Int Symp EUROCK: 21-26

Kataoka M, Obara Y, Kuruppu M (2011) Estimation of fracture toughness of anisotropic rocks by SCB test and visualization of fracture by means of X-ray CT. Proc 12th ISRM Int Cong, Beijing: 667-670

Kuruppu MD, Obara Y, Ayatollahi MR, Chong KP, Funatsu T (2014) ISRM-suggested method for determining the mode I static fracture toughness using semi-circular bend specimen. Rock Mech Rock Eng 47: 267-274

Lee SE, Cho SH, Seo YS, Yang HS, Park HM (2001) The effect of microcracks on the mechanical anisotropy of granite. Materials Sci Res Int 7: 7-13

Meredith PG, Atkinson BK (1985) Fracture toughness and subcritical crack growth during high-temperature tensile deformation of Westerly granite and Black gabbro. Phys Earth Planet Int 39: 33-51

Mukunoki T (2013) Proc 4th Int Workshop on X-ray CT Visualization for Socio-Cultural Eng & Environmental Materials X-Earth

Nasseri MHB, Mohanty B (2008) Fracture toughness anisotropy in granitic rocks. Int J Rock Mech Min Sci 45: 167-193

Obara Y, Sasaki K, Matusyama T, Yoshinaga T (2006) Influence of water vapor pressure of surrounding environment on fracture toughness of rocks. Proc CD 4th ARMS, Singapore: Chap 7

Obara Y, Sasaki K, Yoshinaga T (2007) Influence of water vapor pressure of surrounding environment on fracture toughness and crack velocity of rocks. Proc 11th ISRM Int Cong, Lisbon: 51-54

Ouchterlony F (1980) A new core specimen for the fracture toughness testing of rocks. Swedish Detonic Research Foundation Rep DS, Stockholm

Ouchterlony F (1981) Extension of the compliance and stress intensity formulas for the single edge crack round bar in bending. ASTM STP 745: 237-256

Schedl A, Kronenberg AK, Tullis J (1986) Deformation microstructures of Barre granite: an optical SEM and TEM study. Techtonophysics 122: 149-164

Tutluoglu L, Keles C (2011) Mode I fracture toughness determination with straight notched disk bending method. Int J Rock Mech Min Sci 48: 1248-1261

Whittaker BN, Shingh RN, Sun G (1992) Rock fracture mechanics: principles, design, and applications (developments in geotechnical engineering). Elsevier

Minami Kataoka, Yuzo Obara, Mahinda Kuruppu

Estimation of fracture toughness of anisotropic rocks by semi-circular bend (SCB) test under water vapor pressure

List of figures

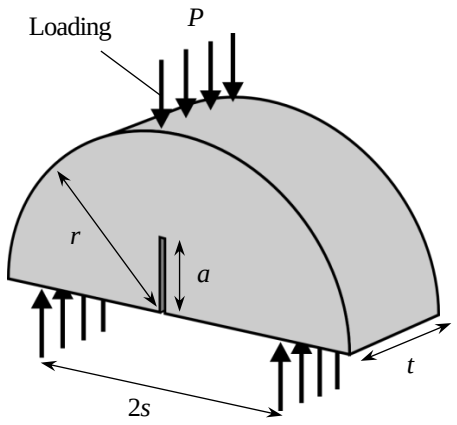

Fig. 1 Semi-Circular Bend (SCB) specimen and loading configuration

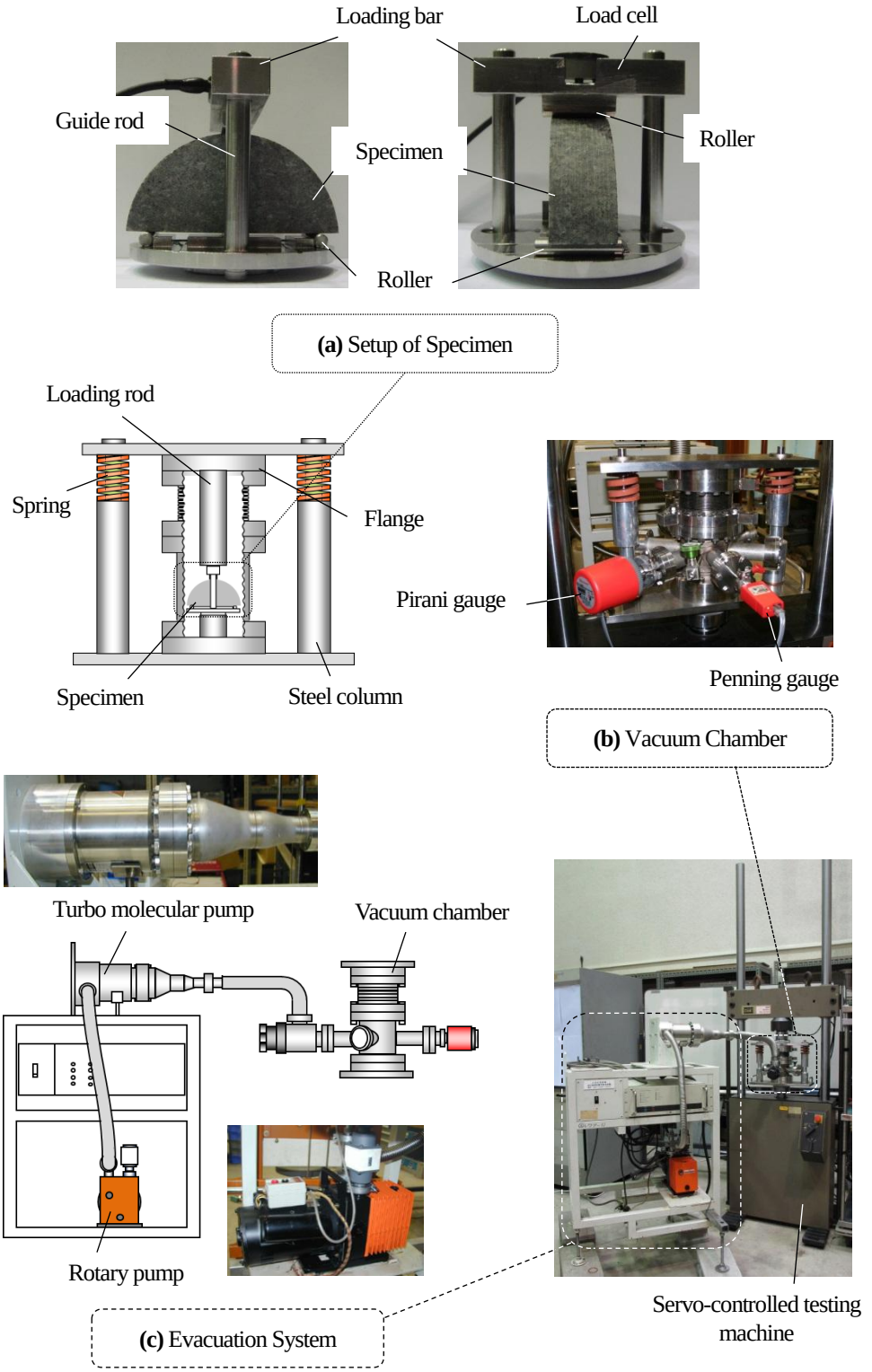

Fig. 2 Testing system: **a** Setup of specimen with loading apparatus placed inside the vacuum chamber, **b** Vacuum chamber used to control surrounding environment of specimen, and **c** Evacuation system consisting of rotary pump and turbo molecular pump (Kataoka and Obara 2013)

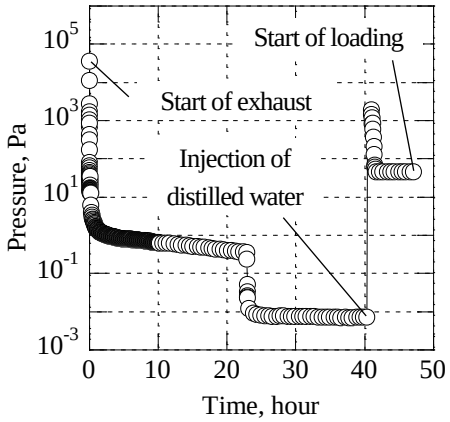

Fig. 3 Change of pressure in the chamber before and during the loading (Kataoka and Obara 2013)

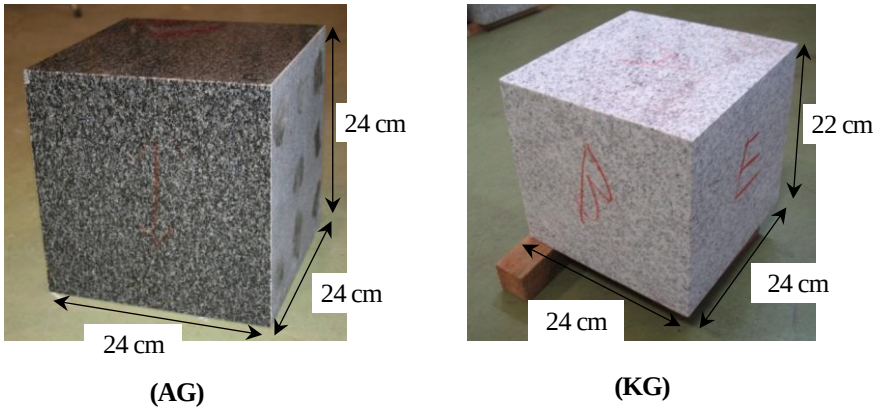

(AG) **(KG)**

Fig.4 Blocks of: **AG** African granodiorite and **KG** Korean granite

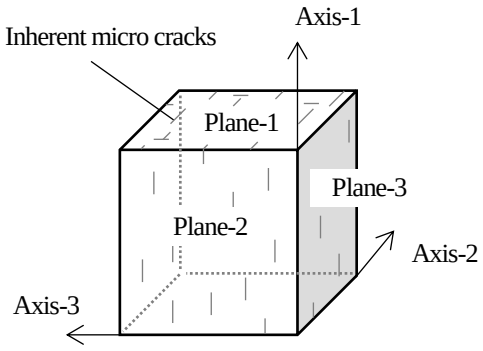

Fig. 5 Definition of axes and planes of rock block and schematic of inherent micro crack distribution

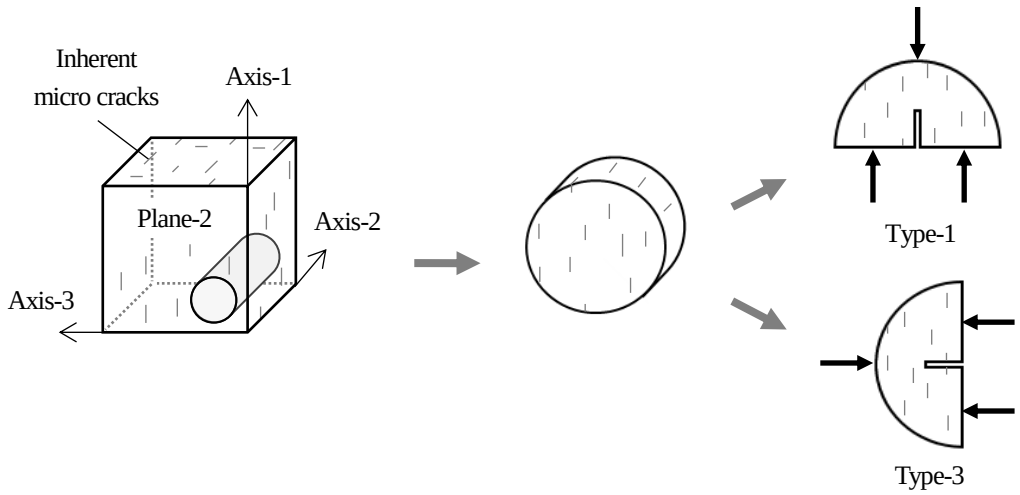

Fig. 6 Schematic of preparation process for obtaining two types of specimens

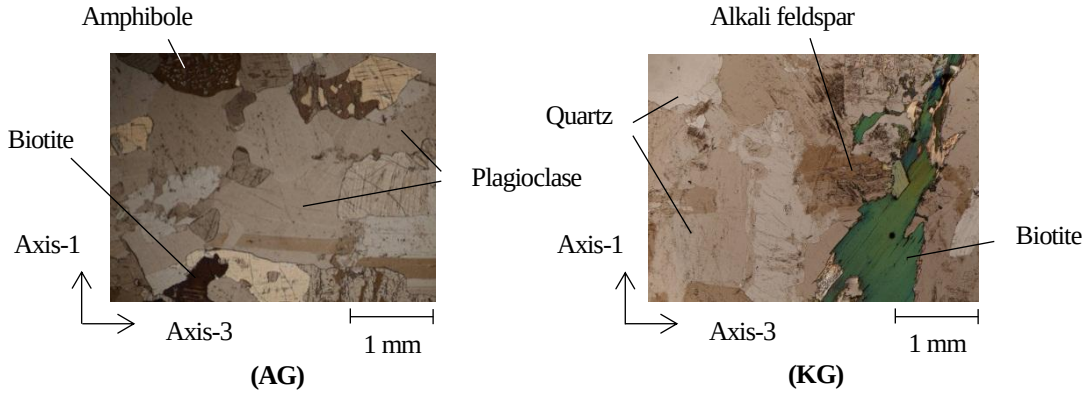

Fig. 7 Micrographs of thin sections (crossed niclos) in Plane-2 for: **AG** African granodiorite and **KG** Korean granite (Kataoka and Obara 2013)

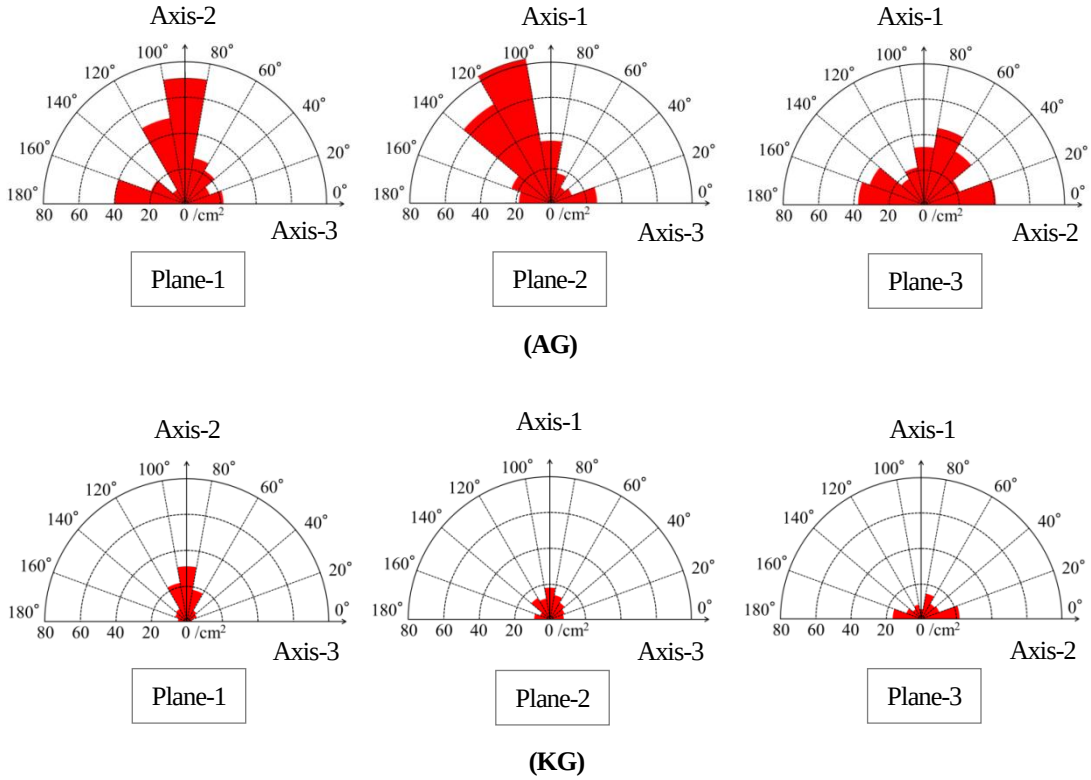

Fig. 8 Micro crack density in Rose diagram for: **AG** African granodiorite and **KG** Korean granite

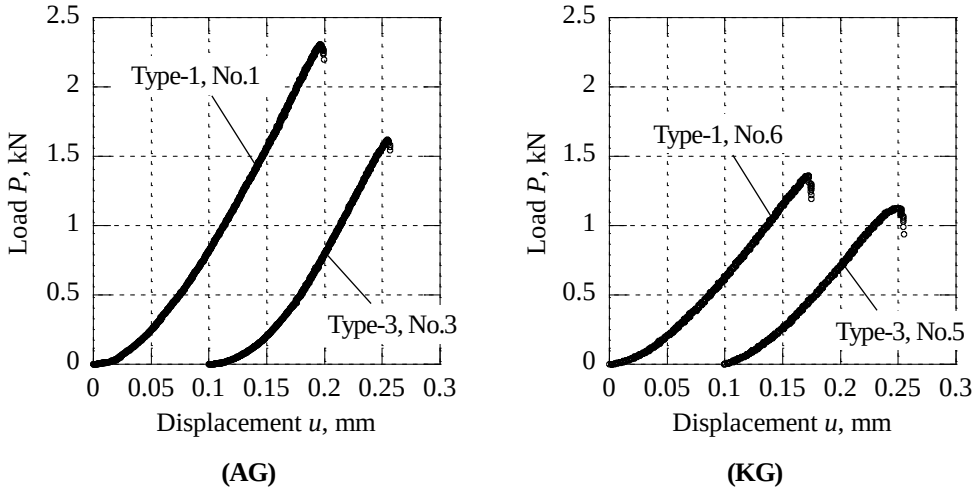

Fig. 9 Load-displacement curves of: **AG** African granodiorite and **KG** Korean granite

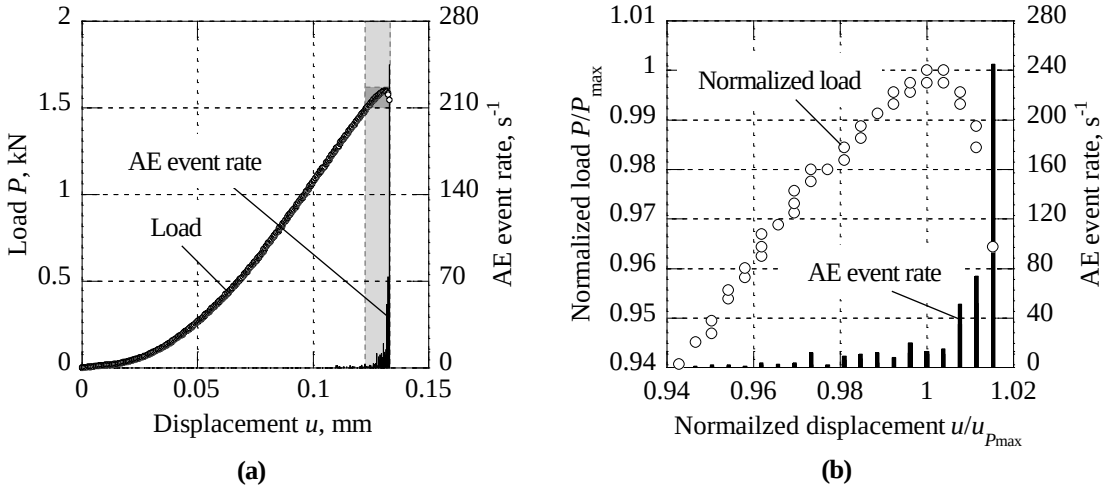

Fig. 10 SCB test results of African granodiorite with AE monitoring: **a** Load and AE event rate vs. displacement, and **b** AE event rate and normalized load vs. normalized displacement. The load and the displacement shown in dark and light grey areas in **Fig. 10 a** are given in **Fig. 10 b** using normalized scales along with the AE event rate

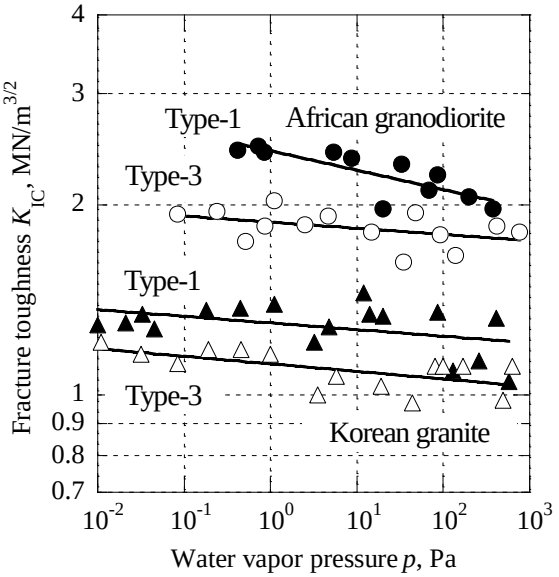

Fig. 11 Relation between fracture toughness and water vapor pressure

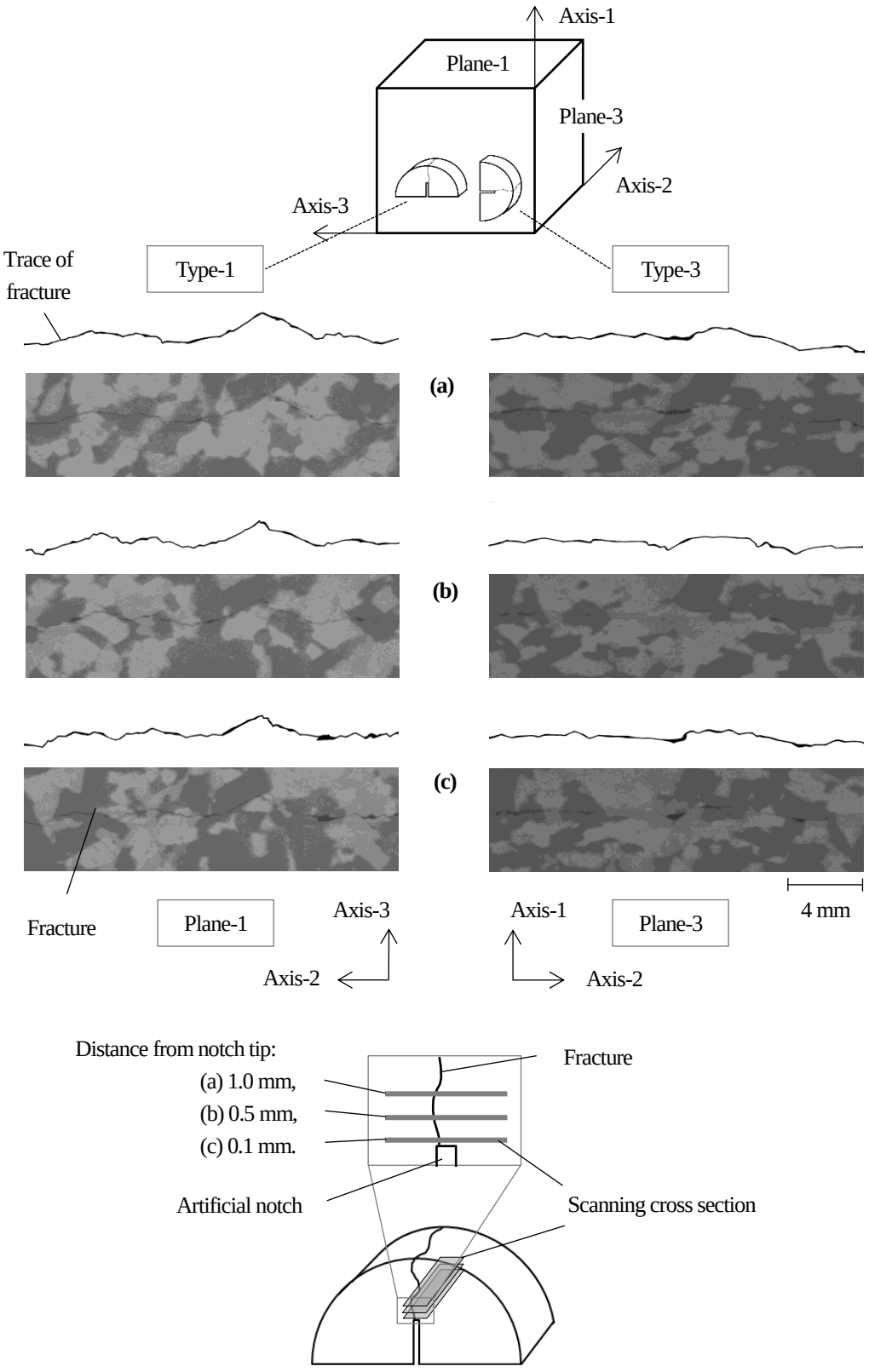

Fig. 12 CT scanned images of fractured specimens of African granodiorite obtained at: **a** 1.0 mm, **b** 0.5 mm, and **c** 0.1 mm distance from the artificial notch tip. Note that the width of each image is equal to the thickness of the specimen

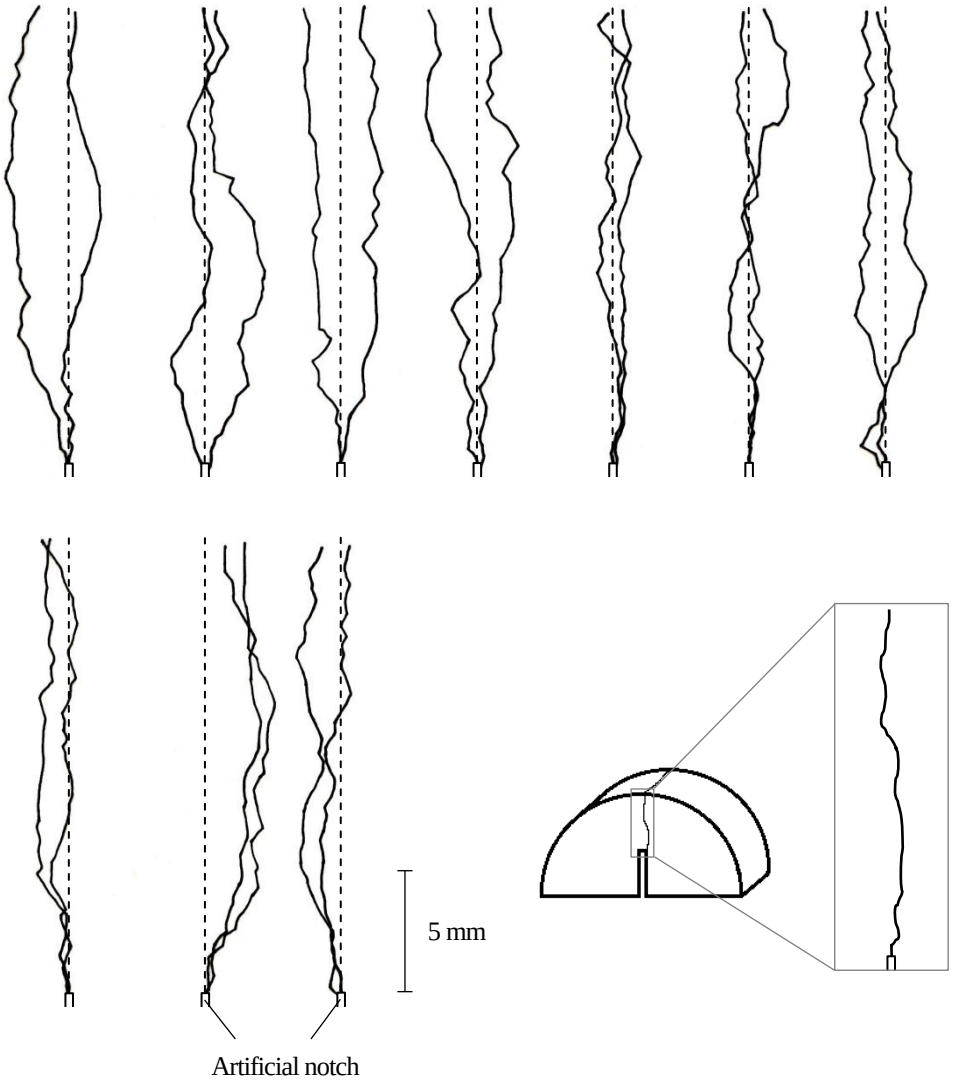

(a) Type-1

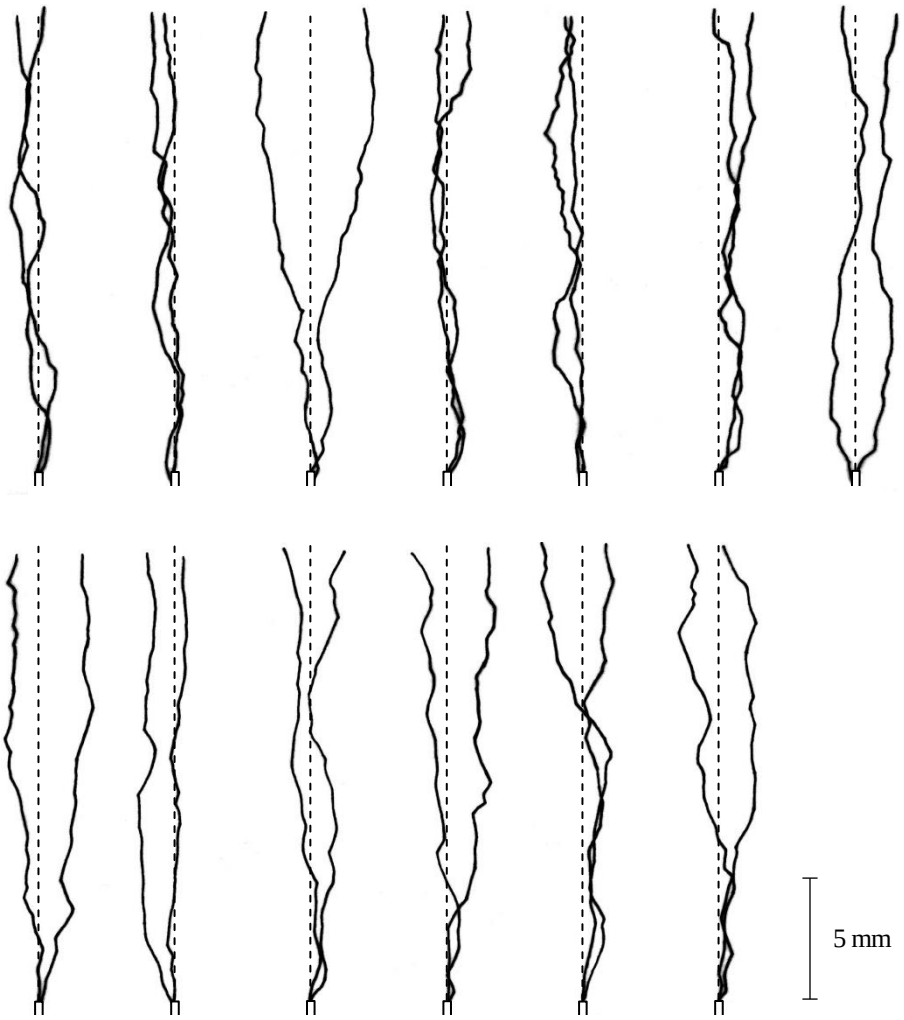

(b) Type-3

Fig. 13 Traces of fractures observed on specimen surfaces of African granodiorite: **a** Type-1 and **b** Type-3

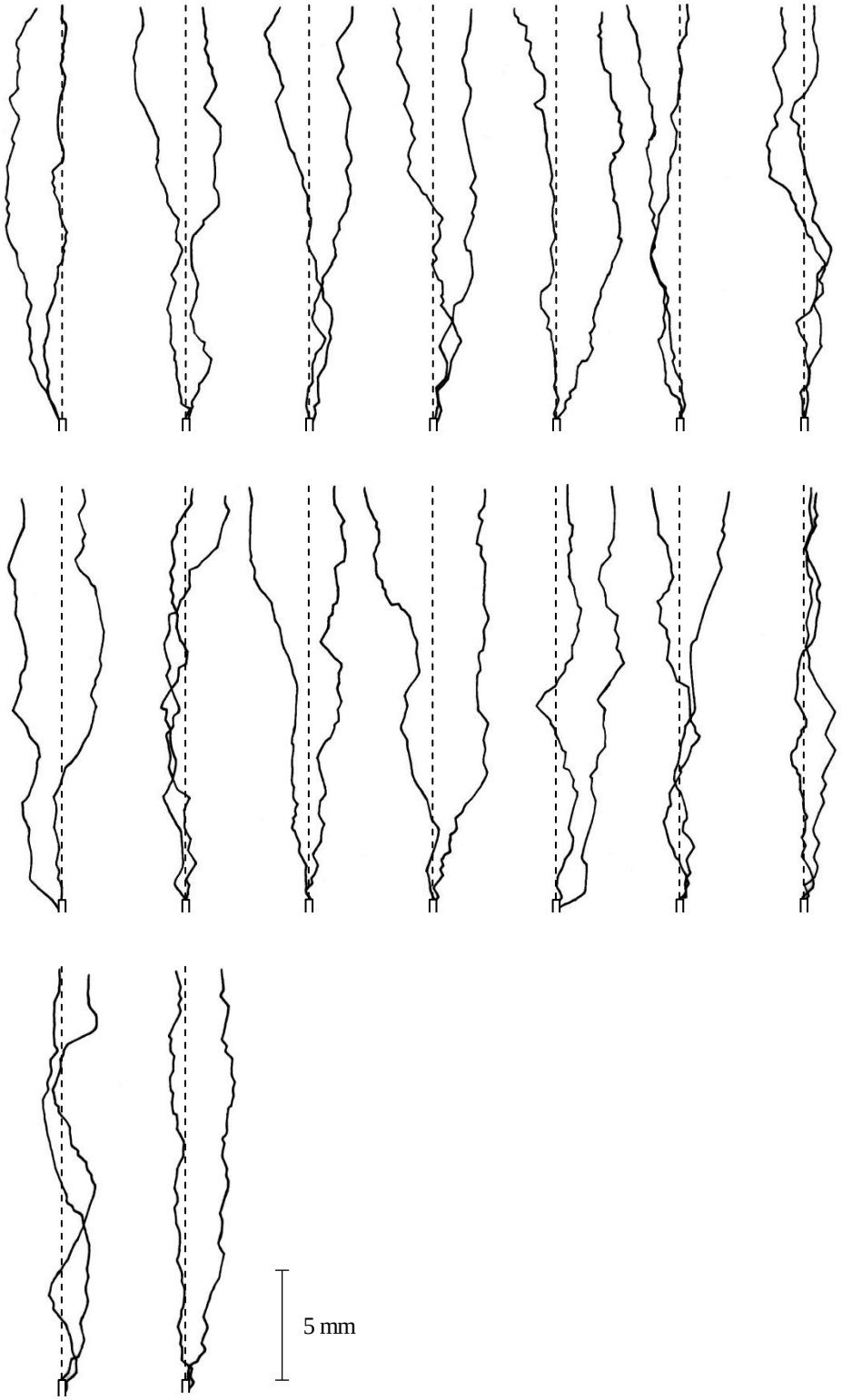

(a) Type-1

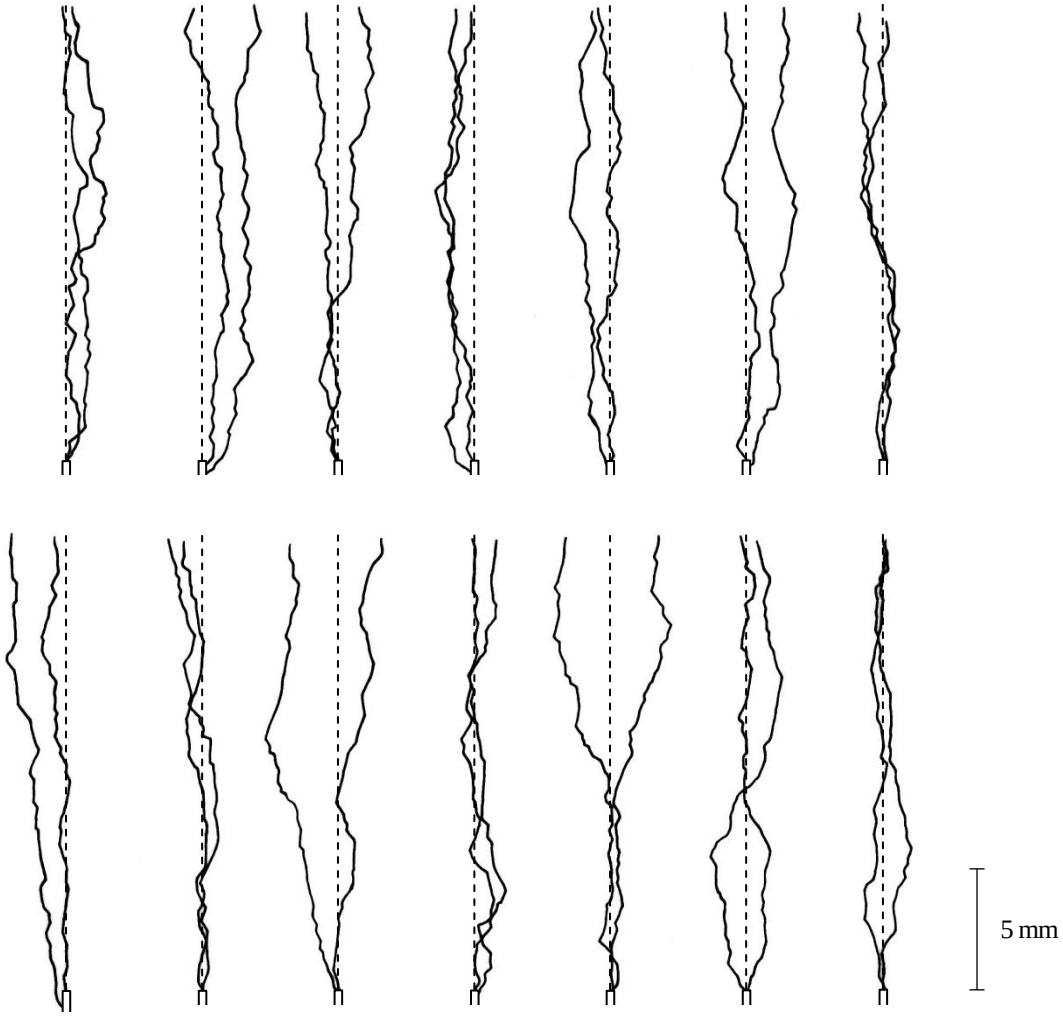

(b) Type-3

Fig. 14 Traces of fractures observed on specimen surfaces of Korean granite: **a** Type-1 and **b** Type-3

Minami Kataoka, Yuzo Obara, Mahinda Kuruppu

Estimation of fracture toughness of anisotropic rocks by semi-circular bend (SCB) test under water vapor pressure

List of tables

Table 1 Elastic wave velocity in the directions of defined axes

	Elastic wave velocity v_p (m/s)		
	Axis-1	Axis-2	Axis-3
African granodiorite	6760	6580	6540
Korean granite	3990	3850	3640

Table 2 Average grain diameters of: **AG** African granodiorite and **KG** Korean granite (Kataoka and Obara 2013)

(AG) African granodiorite

Plane	Direction	Average grain diameter *d* (mm)	Aspect ratio
Plane-1	Axis-2	0.57	1.5
	Axis-3	0.84	
Plane-2	Axis-1	0.62	1.3
	Axis-3	0.80	
Plane-3	Axis-1	0.79	1.1
	Axis-2	0.88	

(KG) Korean granite

Plane	Direction	Average grain diameter *d* (mm)	Aspect ratio
Plane-1	Axis-2	0.66	1.2
	Axis-3	0.76	
Plane-2	Axis-1	0.69	1.0
	Axis-3	0.68	
Plane-3	Axis-1	0.73	1.2
	Axis-2	0.63	

Table 3 Results of SCB tests for African granodiorite: **a** Type-1 and **b** Type-3 (Kataoka and Obara 2013)

(a) Type-1

No.	p (Pa)	r (mm)	t (mm)	a (mm)	Y_I	P_{max} (kN)	K_{IC} (MN/m$^{3/2}$)
1	4.2×10^{-1}	36.7	20.3	17.9	6.63	2.31	2.44
2	7.2×10^{-1}	35.2	21.6	16.3	6.60	2.52	2.48
3	8.5×10^{-1}	36.6	20.2	18.1	6.75	2.22	2.42
4	5.4×10^{0}	37.1	20.2	18.5	6.71	2.23	2.42
5	8.7×10^{0}	36.3	17.8	17.5	6.65	1.96	2.37
6	1.6×10^{1}	36.4	19.9	17.9	6.71	1.80	1.97
7	3.3×10^{1}	36.3	21.5	17.6	6.65	2.32	2.32
8	6.9×10^{1}	36.4	20.3	17.8	6.68	1.98	2.11
9	8.7×10^{1}	35.2	19.0	16.4	6.65	1.97	2.23
10	2.0×10^{2}	35.4	20.1	16.9	6.73	1.89	2.06
11	3.8×10^{2}	36.3	19.0	17.6	6.66	1.73	1.97

(b) Type-3

No.	p (Pa)	r (mm)	t (mm)	a (mm)	Y_I	P_{max} (N)	K_{IC} (MN/m$^{3/2}$)
1	8.4×10^{-2}	36.2	20.1	17.5	6.68	1.79	1.93
2	2.4×10^{-1}	35.6	17.2	17.2	6.76	1.52	1.95
3	5.2×10^{-1}	36.3	20.1	17.6	6.68	1.62	1.75
4	8.6×10^{-1}	36.7	18.9	18.3	6.75	1.59	1.85
5	1.1×10^{0}	36.4	19.6	17.9	6.71	1.82	2.03
6	2.5×10^{0}	36.1	19.7	17.3	6.63	1.71	1.86
7	4.7×10^{0}	35.7	18.7	16.6	6.55	1.71	1.92
8	1.5×10^{1}	36.1	21.2	17.6	6.73	1.75	1.81
9	3.5×10^{1}	35.8	17.1	17.1	6.65	1.28	1.62
10	4.8×10^{1}	36.4	19.6	17.6	6.65	1.76	1.94
11	9.3×10^{1}	35.8	19.9	17.0	6.63	1.66	1.79
12	1.4×10^{2}	36.1	19.9	17.6	6.73	1.51	1.66
13	4.2×10^{2}	36.8	18.9	17.7	6.53	1.67	1.85
14	7.7×10^{2}	35.7	19.0	16.8	6.61	1.61	1.81

p Water vapor pressure, r Radius of specimen, t Thickness of specimen, a Artificial notch length of specimen, Y_I Normalized stress intensity factor, P_{max} Maximum load, K_{IC} Fracture toughness

Table 4 Results of SCB tests for Korean granite: **a** Type-1 and **b** Type-3 (Kataoka and Obara 2013)

(a) Type-1

No.	p (Pa)	r (mm)	t (mm)	a (mm)	Y_I	P_{max} (N)	K_{IC} (MN/m$^{3/2}$)
1	1.0×10^{-2}	37.5	19.6	18.6	6.58	1.18	1.28
2	2.1×10^{-2}	37.5	20.2	18.7	6.63	1.26	1.33
3	3.3×10^{-2}	37.5	20.7	18.9	6.69	1.33	1.40
4	4.5×10^{-2}	37.5	20.6	18.7	6.64	1.26	1.31
5	1.8×10^{-1}	37.5	21.4	18.8	6.66	1.36	1.37
6	4.5×10^{-1}	37.5	21.3	18.7	6.61	1.36	1.36
7	1.1×10^{0}	37.5	19.6	18.6	6.60	1.26	1.36
8	3.2×10^{0}	37.5	20.4	18.8	6.66	1.23	1.30
9	4.8×10^{0}	37.5	20.8	19.0	6.72	1.25	1.31
10	1.2×10^{1}	37.5	18.8	18.8	6.65	1.26	1.44
11	1.4×10^{1}	37.5	20.7	18.9	6.70	1.30	1.37
12	2.0×10^{1}	37.5	20.1	18.8	6.66	1.24	1.34
13	8.7×10^{1}	37.5	20.7	18.7	6.63	1.27	1.32
14	1.3×10^{2}	37.5	21.3	18.4	6.54	1.11	1.09
15	2.6×10^{2}	37.5	20.0	19.0	6.71	1.06	1.16
16	4.1×10^{2}	37.5	20.7	18.9	6.69	1.24	1.31
17	5.8×10^{2}	37.5	18.8	18.9	6.69	0.92	1.06

(b) Type-3

No.	p (Pa)	r (mm)	t (mm)	a (mm)	Y_I	P_{max} (N)	K_{IC} (MN/m$^{3/2}$)
1	1.1×10^{-2}	37.5	21.3	18.3	6.51	1.22	1.20
2	3.2×10^{-2}	37.5	21.3	18.0	6.41	1.18	1.13
3	8.5×10^{-2}	37.5	19.8	18.8	6.66	1.03	1.13
4	1.9×10^{-1}	37.5	21.2	18.8	6.67	1.17	1.19
5	4.6×10^{-1}	37.5	19.9	18.7	6.61	1.13	1.21
6	1.0×10^{0}	37.5	19.8	18.9	6.69	1.09	1.19
7	3.5×10^{0}	37.5	19.1	18.7	6.62	0.91	1.02
8	5.8×10^{0}	37.5	21.3	19.2	6.78	1.07	1.11
9	1.9×10^{1}	37.5	20.2	18.9	6.70	0.98	1.06
10	4.4×10^{1}	37.5	21.4	18.8	6.65	0.98	0.98
11	8.1×10^{1}	37.5	19.3	18.7	6.63	1.05	1.16
12	9.9×10^{1}	37.5	19.4	18.7	6.63	1.00	1.11
13	1.7×10^{2}	37.5	21.3	18.5	6.56	1.15	1.14
14	4.9×10^{2}	37.5	21.6	18.6	6.60	1.00	0.98
15	6.3×10^{2}	37.5	21.3	18.8	6.65	1.10	1.11

p Water vapor pressure, r Radius of specimen, t Thickness of specimen, a Artificial notch length of specimen, Y_I Normalized stress intensity factor, P_{max} Maximum load, K_{IC} Fracture toughness

Table 5 Parameters of lines shown in **Fig 11** (refer to Eq. 2)

	Type	β	m
African granodiorite	1	2.43	0.0301
	3	1.88	0.0102
Korean granite	1	1.32	0.0119
	3	1.13	0.0098

Table 6 Fracture angles: Angle of fracture making with dashed line as shown in **Figs. 13** and **14**

	Type	Average $\pm$ Standard deviation (degrees)
African granodiorite	1	9.7 ± 6.3
	3	6.4 ± 4.7
Korean granite	1	11.7 ± 5.0
	3	7.7 ± 4.3